HHS Public Access

Author manuscript

ACS Appl Mater Interfaces. Author manuscript; available in PMC 2018 December 19.

Published in final edited form as:

ACS Appl Mater Interfaces. 2018 May 02; 10(17): 14509–14516. doi:10.1021/acsami.8b02530.

CaZnOS:Nd^{3+} Emits Tissue-Penetrating near-Infrared Light upon Force Loading

Lejing Li[†], **Lothar Wondraczek**[‡], **Lihua Li**[†,§], **Yu Zhang**[§], **Ye Zhu**[‖], **Mingying Peng**[†,*], and **Chuanbin Mao**[‖,⊥,*]

[†]The China-Germany Research Center for Photonic Materials and Devices, The State Key Laboratory of Luminescent Materials and Devices, Guangdong Provincial Key Laboratory of Fiber Laser Materials and Applied Techniques, School of Materials Science and Technology, South China University of Technology, Guangzhou 510640, P. R. China

[‡]Otto Schott Institute of Materials Research, University of Jena, Jena 07743, Germany

[§]Guangdong Key Lab of Orthopedic Technology and Implant, Department of Orthopedics, Guangzhou General Hospital of Guangzhou Military Command, Guangzhou 510010, P. R. China

[‖]Department of Chemistry and Biochemistry, Stephenson Life Sciences Research Center, University of Oklahoma, Norman, Oklahoma 73019, United States

[⊥]School of Materials Science and Engineering, Zhejiang University, Hangzhou 310027, Zhejiang, P. R. China

Abstract

Mechanoluminescent (ML) materials are mechano-optical converters that can emit light under an external mechanical stimulus. All the existing ML materials can only emit light from near ultraviolet to red, which is outside the near-infrared (NIR) windows desired for biomechanical imaging. No studies have been done on doping rare earth (RE) ions with photoluminescence (PL) in the NIR region into a compound to form a ML material that emits NIR light in response to an external force. Here, we show that doping RE ions with a NIR PL into an inorganic compound does not usually result in the formation of a NIR ML material, which can only be achieved in the combination of Nd^{3+} ions and a CaZnOS compound among the combinations we studied. The newly discovered NIR ML material (CaZnOS:Nd^{3+}) is biocompatible and can efficiently convertmechanical stress into NIR light over the first and second tissue-penetrating bioimaging window. Its NIR ML emission appeared at a very low force threshold (even when the material was shaken slightly), increased sensitively and linearly with the increase in the force (up to >5 kN), and could penetrate the tissue as deep as >22 mm to enable biomechanical detection. Such a force-

[*]**Corresponding Authors:** pengmingying@scut.edu.cn (M.P.). cbmao@ou.edu (C.M.).

Supporting Information

The Supporting Information is available free of charge on the ACS Publications website at DOI: 10.1021/acsami.8b02530. Overview of the existing ML materials, PL of CaZnOS:RE^{3+} (RE^{3+} = Ho^{3+}, Pr^{3+}, Dy^{3+}) materials, NIR PL spectra of $SrAl_2O_4$:Nd^{3+}, ML intensity of CaZnOS:Nd^{3+} compared with the currently reported most efficient visible ML phosphor, and in vitro cytotoxicity experiments (PDF)

The authors declare no competing financial interest.

responsive behavior is highly reproducible. Hence, CaZnOS:Nd^{3+} is a new potential ultrasensitive biomechanical probe and expands the ML application horizons into in vivo bioimaging.

Graphical Abstract

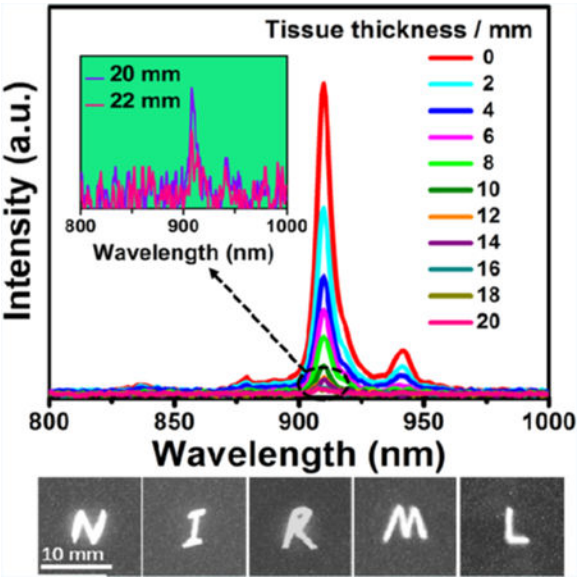

Keywords

CaZnOS:Nd^{3+}; mechanoluminescence; near infrared; tissue penetration; bioimaging; biomechanics

INTRODUCTION

Photoluminescence (PL) uses photons as an excitation source to emit lower-energy photons (down-converted luminescence) or higher-energy photons (up-converted luminescence).[1,] Light is also considered as a reliable signal for in vivo imaging. Either the near-infrared (NIR) persistent luminescence or up-conversion luminescence has been systematically researched and proved as an efficient tool for biological labeling, bioimaging, or solar energy utilization.[3–6] Unlike PL, mechanoluminescence (ML) relies on mechanical stimuli to activate the luminescence process.[7–9] This includes direct mechanical excitation as well as mechanical acceleration of band depopulation in an otherwise excited state.[10] This unique energy conversion process enables ML materials to sense ubiquitous and invisible stress. Monitoring and sensing dynamic mechanical change of the tissues or implants in noninvasive manner remains a challenging task. The ML material is a potential probe to overcome this difficulty, although this has never been demonstrated before. This is mainly because detecting ML emitted from inside a tissue requires the ML to be within the tissue-penetrating near-infrared (NIR) region. Information provided by NIR ML monitoring can aid the design of orthopedic devices, guide fixations, implant alignment, kinematics, joint loading,[11,12] and other interaction situations, so as to complement invasive techniques[13] and indirect or ex situ data from finite-element modeling,[14] and electrometric or photoelastic

analyses.[15,16] But such NIR ML materials have never been discovered. All the existing ML materials can only emit light from the near ultraviolet to the visible (vis) range (Figure S1).

Materials exhibiting ML upon elastic deformation (elastic ML, EML) are of major interest[17,18] because they promise applicability in reliable, nondestructive, and reproducible real-time observation of mechanical change. Monitoring dynamic variations in EML intensity and/or the lateral distribution of an EML signal enables one-, two-, or even three-dimensional (1D, 2D, or 3D) access to stress fields.[19,20] However, ML, in particular, EML, has not been considered suitable for bioimaging because none of the current ML materials can emit NIR lights, in particular, those within the first (650−950 nm) or second (1000−1400 nm) window that are “transparent” for biological samples.

To design such NIR ML materials, we considered two related aspects.[21] One is to find a suitable host lattice for a dopant with the desired emission color, and another is to control luminescence quenching and energy-level mismatch, which determine the occurrence of the desired EML phenomenon. Hence, we chose a combination of the piezoelectric semiconductor CaZnOS with the rare earth (RE) species[22–24] (i.e., Nd^{3+}). CaZnOS was selected as a host lattice due to its proven capacity to dissolve RE^{3+} species and its high piezoelectric coefficient (d_{33} = 38 pm/V)[25] desired as a carrier with de-trapping in EML.[26] It should be noted that using piezoelectric compound as a host is not a mandatory requirement to achieve ML. For example, the nonpiezoelectric compound, $Sr_2SnO_4:Sm^{3+}$, has been used to form ML materials.[27]

On the other hand, although the mechanism of ML is not fully clear, it is hard for the doped emitting ions alone to be excited by external mechanical stimuli. Some energy-level transitions are often missing in ML even if the emitting center can be successfully activated by a PL excitation process.[21] For example, as shown in Figure S2, we found that the PL spectrum excited by ultraviolet or blue light is consistent with the ML spectrum in $CaZnOS:RE^{3+}$ (RE^{3+} = Ho^{3+}, Pr^{3+}, Dy^{3+}) in the range from 450 to 850 nm. However, the compounds $CaZnOS:RE^{3+}$ with these dopants (RE^{3+} = Ho^{3+}, Pr^{3+}, Dy^{3+}) do not present the NIR ML even though they show NIR PL (activated by short-wavelength light). Namely, the compound doped with these RE ions capable of emitting NIR PL do not show NIR ML. This phenomenon was also observed in $SrAl_2O_4:Nd^{3+}$ (Table 1 and Figure S3). Although we did not observe NIR ML when Nd^{3+} was doped in $SrAl_2O_4$ and $SrSnO_3$, surprisingly, we observed NIR ML when CaZnOS was doped with the Nd^{3+} ions, which are one of the most studied NIR PL species.[28–30] Indeed, we observed efficient NIR EML in $CaZnOS:Nd^{3+}$, with a response sensitivity at a comparably low force threshold, an unusual high ML efficiency, a large region of linearity up to >5 kN, and a high cycling stability. Besides, the ML intensity of $CaZnOS:Nd^{3+}$ is 5 times greater than that of the well-known most efficient ML material ($SrAl_2O_4:Eu^{2+},Dy^{3+}$) under 3000 N (Figure S4). We demonstrated that the resultant NIR EML, in the biological window of 650−1400 nm, can be used to penetrate and image tissues with a high sensitivity.

EXPERIMENTAL SECTION

Sample Preparation.

All the compounds were made by a solid-state reaction method using 99.99% pure chemicals $CaCO_3$, ZnS, and Nd_2O_3 as starting materials at high temperature. Specifically, stoichiometric mixtures were first weighed according to the composition CaZnOS:xNd^{3+} (x = 0.05, 0.1, 0.2, 0.5, 1.0, and 2.0 mol %) and then ground and mixed homogeneously in an agate mortar. Parts of the mixed samples were shaped and pressed into disks with a diameter of 20 mm using an isostatic pressing machine (8 MPa) for later tribological ML (tribo-ML) measurements. Mixed powder and tablet samples were then sintered in alumina crucibles at 1000 °C for 3 h using a horizontal tube furnace under flowing argon (35 mL/min). The sintered powder samples were subsequently ground again into fine powders, which were subsequently dispersed into transparent epoxy resin (SpeciFix, Struers GmbH) with different ratios for ML experiments. For compression ML (com-ML), cylindrical composite samples were made into a disk (25 mm in diameter and 15 mm in thickness) by mixing CaZnOS: 0.5% Nd^{3+} and transparent epoxy resin under a mass ratio of 1:9. For tribo-ML and 2D handwriting experiments, phosphor wafers were made into pellets (25 mm in diameter and 5 mm in thickness) by mixing CaZnOS:0.5% Nd^{3+} and resin at a weight of 1:3. The commercial phosphor $SrAl_2O_4$:Eu^{3+},Dy^{3+} was purchased and mixed with as-prepared CaZnOS:0.5% Nd^{3+} at the mole ratio of 1:1, then the mixed ML phosphor was embedded into resin to form the composite testing sample with the same size mentioned above.

Characterization.

X-ray diffraction (XRD) and scanning electron microscopy coupled with energy-dispersive X-ray (EDX) spectroscopy were used to characterize the phase structures, as well as the particle size and composition of the samples. Static fluorescence excitation and emission spectra, emission decay, and time-resolved spectra were recorded with an Edinburgh FLS 920 spectrofluorometer equipped with a red-sensitive photomultiplier (Hamamatsu R928P). A microsecond pulsed xenon flash lamp μF900 (60 W) and a ozone-free xenon lamp (450 W) were utilized as an excitation source for the emission decay and the steady-state measurements, respectively. For com-ML and tribo-ML, stresses were loaded with a universal testing machine (WEW 600, Shenzhen SUNS Technology Stock Co., LTD) and a homemade setup, respectively. It is worth mentioning that for the loading and release cycling experiments, the samples were illustrated for 10 s by a 365 nm lamp during each interval. Com-ML and tribo-ML spectra were collected by Ocean fiber spectrometers QE65pro and NIRQuest512, respectively.

To evaluate the optical transmittance of the ML signal from CaZnOS:0.5% Nd^{3+} through biological tissue, a setup was built and is illustrated in Results and Discussion. The NIR tribo-ML photons were induced by a stainless-steel tip from the sample mounted on a platform, which was motor driven at a speed of 1600 rpm. The NIR ML photons emitted from the sample went through the hole and were collected by a digital NIR camera (Goldeye P-008 SWIR, Allied Vision Technologies) and a fiber optical spectrometer (QE65pro, Ocean Optics), respectively. The multimode fiber pigtailed to the Ocean Optics spectrometer was 1.2 m long with a numerical aperture of 0.22. Pork slices, each of which was ~2 mm think,

covered the hole right on top of the phosphor sample. The thickness of the tissues was controlled by the number of slices stacked. A silicate glass rod with a diameter of 3 mm was used to write on the phosphor wafer sample, and the 2D planar handwriting mapping was recorded with the abovementioned NIR camera with an exposure time of 2 s. A sintered cylindrical sample (15 mm in diameter and 10 mm in thickness) was wrapped by polyethylene film. Then, the sample was put into mouth and bitten by the teeth. The sample remained intact after suffering from tooth occlusion. All the NIR ML spectra from open mouth and close mouth were collected by the Ocean fiber spectrometers QE65pro with a fiber against the mouth. Three-dimensional thermoluminescence (ThL) spectra were obtained on an instrument made up of a charge-coupled device (CCD) detector and a heating stage on which the sample was heated from room temperature to 503 K at a heating speed of 3 K/s. The ThL data were the integral intensity in a spectrum range of 800−1000 nm as a function of temperature.

Cell Proliferation.

The proliferation of the cells (mouse fibroblast cell line L929 cells, human umbilical vein endothelial cells (HUVECs), and mouse preosteoblast cells (MC3T3-E1)) on different concentrations of sample particles was evaluated using 3-(4,5-dimethylthiazol-2-yl)-diphenyltetrazolium bromide (MTT) assay.

RESULTS AND DISCUSSION

X-ray diffraction (XRD) from a series of CaZnOS:Nd^{3+} (Figure 1a) shows that doping with Nd^{3+} ions does not cause significant changes in the crystalline lattice. However, a closer inspection (Figure 1b) reveals a shift in the strongest diffraction peak toward a higher angle, indicating a lattice shrinkage with an increase in the dopant content. Such a shrinkage is expected because the slightly smaller Nd^{3+} ions (CN6, 0.98 Å) replace the larger Ca^{2+} ions (CN6, 1.00 Å). The energy-dispersive X-ray (EDX) spectroscopic mapping on a randomly selected sample of CaZnOS:2.0% Nd^{3+} (Figure 1c, particle size ~ 3 μm) confirms a highly homogeneous distribution of the Nd^{3+} dopant within a particle.

Under external mechanical stimuli such as compressing or rubbing of the CaZnOS:0.5% Nd^{3+} samples in the compression or tribology experiments (Figure 2a), the samples emitted intense NIR EML emission (denoted as com-ML or tribo-ML, respectively). In particular, three main emission peaks, located at 890−950, 1050−1150, and 1350−1400 nm, can be traced in each spectrum, corresponding to the transitions of Nd^{3+} from $^4F_{3/2}$ to $^4I_{9/2}$, $^4I_{11/2}$, and $^4I_{13/2}$, respectively. The weak satellite peaks near each of the main bands might arise from the Stark splitting in the crystal field of CaZnOS.

To apply CaZnOS:Nd^{3+} materials to force and stress sensing, response sensitivity and linearity are key parameters under a mechanical stimulus and thus were studied. The NIR com-ML intensity was linearly increased with an increase in load (Figure 2b,c). The force threshold should be much lower than the observed 100 N because we could still detect the emission as we gently touched the sample surface with a glass rod or slightly shook it within a beaker. To gain an insight into the ML properties of CaZnOS:Nd^{3+} for long time use, compressive force cycles between 0 and 1000 N was applied to the samples. The EML

intensity decreased significantly under the same consecutive load cycle with unchanged emission spectra, and integrated intensity of EML under the tenth load was about 5% that of the initial ML peak intensity (Figure 2d,e). However, as shown in Figure 2f, the EML phenomenon displays a typical recoverable performance after being charged by UV irradiation. The integrated intensity of EML grew when the force was increased but attenuated sharply after load removal (Figure 2f). This recoverable EML properties almost keep stable after six cycles of repeated UV-charging and -loading. These results demonstrate that the EML is attributable to a trap-controlled luminescence process. The electrons were released from traps as an external consecutive load was applied to the sample, leading to attenuated NIR ML intensity. However, the traps were refilled when the sample was exposed to high-energy photons such as UV irradiation, then NIR ML was recovered as well. Hence, the loading and UV irradiation act as charging and discharging processes, respectively, contributing to the recoverable NIR ML phenomenon. To demonstrate that the EML material can be used as a signature collector for recording abundant personal writing identities,[17] as schematically illustrated in the right part of Figure S1, we used a silicate glass rod as a "pencil" to write the letters "SCUTNIRML" on the same spot of a sintered sheet sample. Then, the glowing trace can be captured by an NIR camera right above the sheet gradually. Surprisingly, the low EML stress threshold of CaZnOS:Nd^{3+} allowed these letters to be displayed on the sample in the order of writing (Figure 2g).

MTT assay showed that CaZnOS:Nd^{3+} powders were not toxic to mouse and human cells when the concentration was below 500 μg/L (Figure S5), suggesting their excellent biocompatibility.[31] To further prove that the NIR EML from CaZnOS:Nd^{3+} can be used for tissue imaging, we established a setup shown in Figure 3a, where the CaZnOS:Nd^{3+} phosphor is mounted on a rotary platform driven by a motor. Once a stainless-steel tip touched the phosphor surface, the NIR EML would be induced and go through a hole (right above the phosphor) to reach the biological specimen (using pork slices as a tissue model) right above the hole. If the NIR EML could penetrate the tissue, partial EML would reach a digital NIR camera placed above the tissue to form a flash photo. Partial EML would also be collected by a multimode fiber, transmitted through the fiber, and resolved immediately into an emission spectrum by an NIR CCD of a spectrometer. Clearly, strong NIR EML could be visualized by either tissue imaging (Figure 3b) or emission spectra recording (Figure 3c) when the tissue thickness was below 22 mm. As tissue thickness increased, the emission intensity went down correspondingly without a shift in the emission peak (Figure 3b,c). At a thickness of 6 mm, the emission intensity only decreased to one third of the original value in the absence of tissue in the light path. Residual chromophores, refractive index mismatch, enhanced scattering, and absorption might cause the extinction of the incident beam of the NIR photons. Even as the thickness of the tissue became 22 mm, weak NIR EML signals could still be detected at 908 nm (inset in Figure 3c). By plotting logarithmic transmission intensity versus tissue thickness, an extinction coefficient was determined to be −0.124 (Figure 3d).

To demonstrate the application of NIR ML in biomechanical imaging, we examined the NIR ML under biological force. Specifically, we recorded the NIR ML from the sintered cylindrical samples when the samples were bitten by the human teeth. Indeed, we observed a distinct NIR ML signal when the sample was bitten by the teeth but with the mouth open

(left spectra in Figure 3e). When the mouth was closed but the sample was still bitten by the teeth, the NIR ML signal could still be detected (right spectra in Figure 3e). These results indicate that NIR ML could be generated by biological force (i.e., teeth biting) and then pass through the lip tissue of the closed mouth and be detected. It should be noted that no NIR light can be detected when the sample was not bitten by the human teeth. Hence, this ML material can enable high-resolution and real-time visualization of the dynamic mechanical changes in the tissues.

To understand how ML occurred, we measured the PL properties of CaZnOS:Nd^{3+}. The Nd^{3+} ion is known as an efficient NIR luminescence center due to the energy-level transitions from $^4F_{3/2}$ to I_J (J = 9/2, 11/2, 13/2). The PL excitation spectra at the emission wavelengths of 908 and 1094 nm suggested the excitation of NIR emissions over a wide range of vis-NIR light (Figure 4a), with the broad peak in the shorter-wavelength range originating from the fundamental absorption edge of the host. A time-resolved PL spectrum (Figure 4b) showed that with an increase in the delay up to 500 μs, the intensity of Nd^{3+}-related photoemission gradually decreased while maintaining the overall shape of the emission spectrum, indicating there was only one type of Nd^{3+} emission center in CaZnOS:Nd^{3+}. The hexagonal CaZnOS phase has only one type of Ca sites available, which are coordinated by three oxygen atoms and three sulfur atoms. The Ca−O bond is about 0.74 Å shorter than the Ca−S bond. In view of the size and charge matches, Nd should preferentially occupy the Ca sites in CaZnOS:Nd^{3+}. The critical dopant concentration was found to be ~0.2 mol %. The decay curves of the emissions at 908 and 1094 nm well followed a single exponential equation for all the concentrations (Figure 4c). Fitting to the equation produced the lifetimes for each sample. The lifetimes slightly decreased from 125 to 110 μs for the emission at 1094 nm and from 123 to 105 μs for the emission at 908 nm when the dopant content was increased (Figure 4c). This is perhaps due to concentration quenching. For each concentration, we noticed that the lifetimes of the emissions at 1094 and 908 nm were comparable, proving that these emissions originated from the same excited level of $^4F_{3/2}$.

We then measured the 3D thermoluminescence (ThL) spectra to illustrate the possible defect traps inside CaZnOS:Nd^{3+}. A sharp peak was observed at ~908 nm within 800−1000 nm (Figure 4d), consistent with the aforementioned PL spectra. The 3D ThL spectrum also revealed a peak at 108 °C. This peak allowed us to determine a trap depth of ~0.762 eV through Urbath's approximation, $E = T_m/500$,[32] where E is the depth of trap level with a unit of eV and T_m is the peak temperature (K) of the ThL curve.

After light excitation, the electrons of Nd^{3+} ions will be lifted up to the upper excited states from the ground state of $^4I_{9/2}$. The excited electrons after fast nonradiative relaxations return back to the lowest excited state of $^4F_{3/2}$, where they may stay for about 100 μs (Figure 4c). They jump back to $^4I_{9/2}$, $^4I_{11/2}$, and $^4I_{13/2}$ and release the lights at ~908, ~1094, and ~1390 nm, respectively. When an external mechanical stimulus is applied to this host, a local piezoelectric field will be produced and become even higher near the activators or defects. The field may excite Nd^{3+} ions into higher excited states or promote the electron release from electron traps by removing the barrier of the carrier detrapping process. The local piezoelectric field may temporarily narrow the band gap and thus reduce the trap depth.[33]

Therefore, electrons are detrapped and contribute partially to the ML processes. The NIR ML emission attenuated with trapped electrons were emptied by consecutive mechanical stimuli; however, this emission could be fully recovered by UV irradiation (Figure 2f), i.e., traps were filled again by high-energy photons. We believe these charging and discharging processes are responsible for the recoverable NIR ML phenomenon.

All the current EML materials cannot emit NIR ML and thus cannot be used as an ultrasensitive force-responsive probe in bioimaging. It is obvious that the NIR EML CaZnOS:Nd^{3+}materials discovered in this study can serve as optical probes that can monitor the mechanical change in the tissues or implants in a noninvasive manner by simply detecting the tissue-penetrating NIR light. Such a method will complement the currently used invasive diagnosis techniques.[13,34] The human lip is about 1 cm in thickness. Our study shows that the EML induced by biting the CaZnOS:Nd^{3+}disk can pass through the tissue with a thickness of cm scale simply because the induced EML is tissue-penetrating NIR light (Figure 3e).

CONCLUSIONS

In summary, we discovered the NIR EML from a biocompatible phosphor CaZnOS:Nd^{3+}. A combination of the same host (or other hosts) and other RE ions (with or without NIR PL) did not show a NIR EML, suggesting that simply doping RE ions with NIR PL into a compound (either piezoelectric or nonpiezoelectric) will not necessarily generate a NIR EML. The PL, com-ML, and tribo-ML of the CaZnOS:Nd^{3+} phosphor showed identical emission spectra. We proved that there existed a direct linear relationship between compressive stress and EML intensity. We also found that the EML intensity of the phosphor was highly sensitive to external mechanical stimuli. The NIR EML from CaZnOS:Nd^{3+} lies within the spectral window that can deeply penetrate the tissue, enabling the phosphor to serve as a force-sensitive optical probe for future in vivo biomechanical imaging in real time. This work demonstrates a new strategy of designing novel EML materials and expands the potential applications of EML phosphors into biomedical fields.

Supplementary Material

Refer to Web version on PubMed Central for supplementary material.

ACKNOWLEDGMENTS

We acknowledge financial support from the National Natural Science Foundation of China (51672085 and 51673168), Program for Innovative Research Team in University of Ministry of Education of China (IRT_17R38), the Key Program of Guangzhou Scientific Research Special Project (201607020009), National Key Research and Development Plan (2017YFF0104504 and 2016YFA0100900), Fundamental Research Funds for the Central Universities, and the Hundred, Thousand and Ten Thousand Leading Talent Project in Guangdong Program for Special Support of Eminent Professionals. Y.Z. and C.M. would like to acknowledge the support from National Institutes of Health (CA200504, CA195607, and EB021339).

REFERENCES

(1). Sun L; Ge X; Liu J; Qiu Y; Wei Z; Tian B; Shi L Multifunctional Nanomesoporous Materials With Upconversion (in Vivo) and Downconversion (in Vitro) Luminescence Imaging Based on

Mesoporous Capping UCNPs and Linking Lanthanide Complexes. Nanoscale 2014, 6, 13242–13252. [PubMed: 25263544]

(2). Zhang X; Zhao Z; Zhang X; Cordes DB; Weeks B; Qiu B; Madanan K; Sardar D; Chaudhuri J Magnetic and Optical Properties of $NaGdF_4$:Nd^{3+}, Yb^{3+}, Tm^{3+} Nanocrystals with Upconversion/Downconversion Luminescence from Visible to the Near-Infrared Second Window. Nano Res 2015, 8, 636–648.

(3). Abdukayum A; Chen J-T; Zhao Q; Yan X-P Functional Near Infrared-Emitting Cr^{3+}/Pr^{3+} Co-Doped Zinc Gallogermanate Persistent Luminescent Nanoparticles with Superlong Afterglow for in Vivo Targeted Bioimaging. J. Am. Chem. Soc 2013, 135, 14125–14133. [PubMed: 23988232]

(4). Pan Z; Lu Y-Y; Liu F Sunlight-activated long-persistent luminescence in the near-infrared from Cr3+-doped zinc gallogermanates. Nat. Mater 2011, 11, 58–63. [PubMed: 22101812]

(5). Yang Y; Shao Q; Deng R; Wang C; Teng X; Cheng K; Cheng Z; Huang L; Liu Z; Liu X; Xing B In Vitro and in Vivo Uncaging and Bioluminescence Imaging by Using Photocaged Upconversion Nanoparticles. Angew. Chem., Int. Ed 2012, 51, 3125–3129.

(6). Huang X; Han S; Huang W; Liu X Enhancing Solar Cell Efficiency: The Search for Luminescent Materials as Spectral Converters. Chem. Soc. Rev 2013, 42, 173–201. [PubMed: 23072924]

(7). Chandra BP; Chandra VK; Jha P Modelling of Fracto-Mechanoluminescence Damage Sensor for Structures. Sens. Actuators, A 2015, 230, 83–93.

(8). Chandra BP; Baghel RN; Luka AK; Sanodiya TR; Kuraria RK; Kuraria SR Strong Mechanoluminescence Induced by Elastic Deformation of Rare-Earth-Doped Strontium Aluminate Phosphors. J. Lumin 2009, 129, 760–766.

(9). Zhang JC; Xu CN; Kamimura S; Terasawa Y; Yamada H; Wang X An Intense Elastico-Mechanoluminescence Material CaZnOS:Mn^{2+} for Sensing and Imaging Multiple Mechanical Stresses. Opt. Express 2013, 21, 12976–12986. [PubMed: 23736551]

(10). Botterman J; Van den Eeckhout K; Bos AJJ; Dorenbos P; Smet PF Persistent Luminescence in $MSi_2O_2N_2$:Eu Phosphors. Opt. Mater. Express 2012, 2, 341–349.

(11). Besier TF; Gold GE; Beaupr GS; Delp SL A Modeling Framework to Estimate Patellofemoral Joint Cartilage Stress in Vivo. Med. Sci. Sports Exercise 2005, 37, 1924–1930.

(12). Wang Y; Li Z; Wong DW; Zhang M Effects of Ankle Arthrodesis on Biomechanical Performance of the Entire Foot. PLoS One 2015, 10, No. e0134340.

(13). Burr DB; Milgrom C; Fyhrie D; Forwood M; Nyska M; Finestone A; Hoshaw S; Saiag E; Simkin A In Vivo Measurement of Human Tibial Strains During Vigorous Activity. Bone 1996, 18, 405–410. [PubMed: 8739897]

(14). Jaecques SVN; Van Oosterwyck H; Muraru L; Van Cleynenbreugel T; De Smet E; Wevers M; Naert I; Vander Sloten J Individualised, Micro CT-Based Finite Element Modelling as a Tool for Biomechanical Analysis Related to Tissue Engineering of Bone. Biomaterials 2004, 25, 1683–1696. [PubMed: 14697870]

(15). Beaupied H; Lespessailles E; Benhamou CL Evaluation of Macrostructural Bone Biomechanics. Jt., Bone, Spine 2007, 74, 233–239.

(16). Roriz P; Carvalho L; Frazao O; Santos JL; Simoes JA From Conventional Sensors to Fibre Optic Sensors For Strain and Force Measurements in Biomechanics Applications: A Review. J. Biomech 2014, 47, 1251–1261. [PubMed: 24612722]

(17). Wang X; Zhang HL; Yu RM; Dong L; Peng DF; Zhang AH; Zhang Y; Liu H; Pan CF; Wang ZL Dynamic Pressure Mapping of Personalized Handwriting by a Flexible Sensor Matrix Based on the Mechanoluminescence Process. Adv. Mater 2015, 27, 2324–2331. [PubMed: 25711141]

(18). Timilsina S; Lee KH; Kwon YN; Kim JS; Reimanis I Optical Evaluation of In Situ Crack Propagation by Using Mechanoluminescence of $SrAl_2O_4$:Eu^{2+},Dy^{3+} . J. Am. Ceram. Soc 2015, 98, 2197–2204.

(19). Chandra BP; Chandra VK; Mahobia SK; Jha P; Tiwari R; Haldar B Real-time Mechanoluminescence Sensing of the Amplitude and Duration of Impact Stress. Sens. Actuators, A 2012, 173, 9–16.

(20). Yoshida A; Liu L; Tu D; Kainuma S; Xu C-N Mechanoluminescent Testing as an Efficient Inspection Technique for the Management of Infrastructures. J. Disaster Res 2017, 12, 506–514.

(21). Zhang J-C; Long Y-Z; Yan X; Wang X; Wang F Creating Recoverable Mechanoluminescence in Piezoelectric Calcium Niobates through Pr3+ Doping. Chem. Mater 2016, 28, 4052–4057.

(22). Zhang Z-J; Feng A; Chen X-Y; Zhao J-T Photo-luminescence Properties and Energy Levels of RE (RE = Pr, Sm, Er, Tm) in Layered-CaZnOS Oxysulfide. J. Appl. Phys 2013, 114, No. 213518.

(23). Tu D; Xu CN; Fujio Y; Kamimura S; Sakata Y; Ueno N Phosphorescence Quenching by Mechanical Stimulus in CaZnOS:Cu. Appl. Phys. Lett 2014, 105, No. 011908.

(24). Duan CJ; Delsing ACA; Hintzen HT Photo-luminescence Properties of Novel Red-Emitting Mn2+-Activated MZnOS (M = Ca, Ba) Phosphors. Chem. Mater 2009, 21, 1010–1016.

(25). Sambrook T; Smura CF; Clarke SJ Structure and Physical Properties of the Polar Oxysulfide CaZnOS. Inorg. Chem 2007, 46, 2571–2574. [PubMed: 17348643]

(26). Chandra VK; Chandra BP; Jha P Strong Luminescence Induced by Elastic Deformation of Piezoelectric Crystals. Appl. Phys. Lett 2013, 102, No. 241105.

(27). Kamimura S; Yamada H; Xu C-N Strong Reddish-Orange Light Emission from Stress-Activated Srn+1SnnO3n+1:Sm (n= 1, 2, ∞) with Perovskite-Related Structures. Appl. Phys. Lett 2012, 101, 091113.

(28). Campbell JH; Suratwala TI Nd-doped Phosphate Glasses for High-Energy/High-Peak-Power Lasers. J. Non-Cryst. Solids 2000, 263–264, 318–341.

(29). Lu K; Dutta NK Spectroscopic Properties of Nd-Doped Glass for 944 nm Laser Emission. J. Appl. Phys 2001, 89, 3079–3083.

(30). Kumar KU; Babu P; Jang KH; Seo HJ; Jayasankar CK; Joshi AS Spectroscopic and 1.06 μm Laser Properties of Nd^{3+}-doped K–Sr–Al Phosphate and Fluorophosphate Glasses. J. Alloys Compd 2008, 458, 509–516.

(31). Tang F; Li L; Chen D Mesoporous Silica Nanoparticles: Synthesis, Biocompatibility and Drug Delivery. Adv. Mater 2012, 24, 1504–1534. [PubMed: 22378538]

(32). Shalgaonkar CS; Narlikar AV Review: A Review of the Recent Methods for Determining Trap Depth from Glow Curves. J. Mater. Sci 1972, 7, 1465–1471.

(33). Chandra BP; Chandra VK; Jha P Elastico-mechanoluminescence and Crystal-Structure Relationships in Persistent Lumines-cent Materials and II–VI Semiconductor Phosphors. Phys. B 2015, 463, 62–67.

(34). Komi PV Relevance of in Vivo Force Measurements to Human Biomechanics. J. Biomech 1990, 23, 23–34. [PubMed: 2081741]

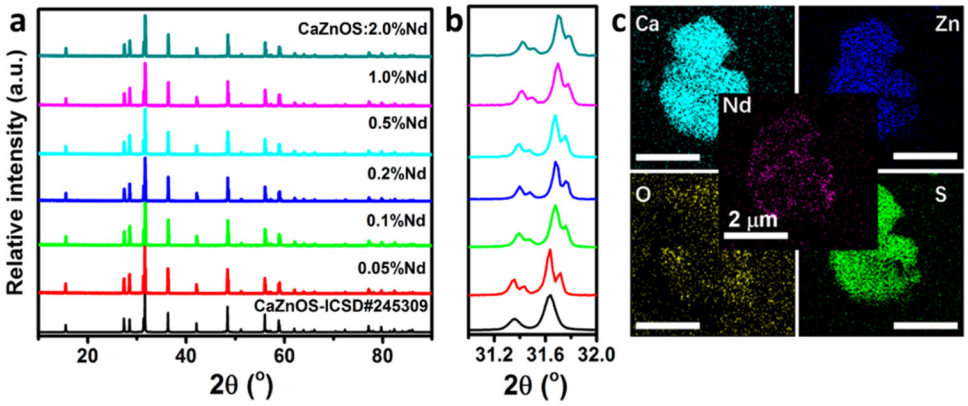

Figure 1.

Crystal structure and morphology of the as-prepared samples. (a) XRD patterns of CaZnOS:Nd^{3+} samples (Nd^{3+} content as indicated, mol %). (b) Magnified 2θ region of 31.0−32.0° in (a). (c) EDX elemental distribution maps of an as-received CaZnOS:2.0% Nd^{3+} particle.

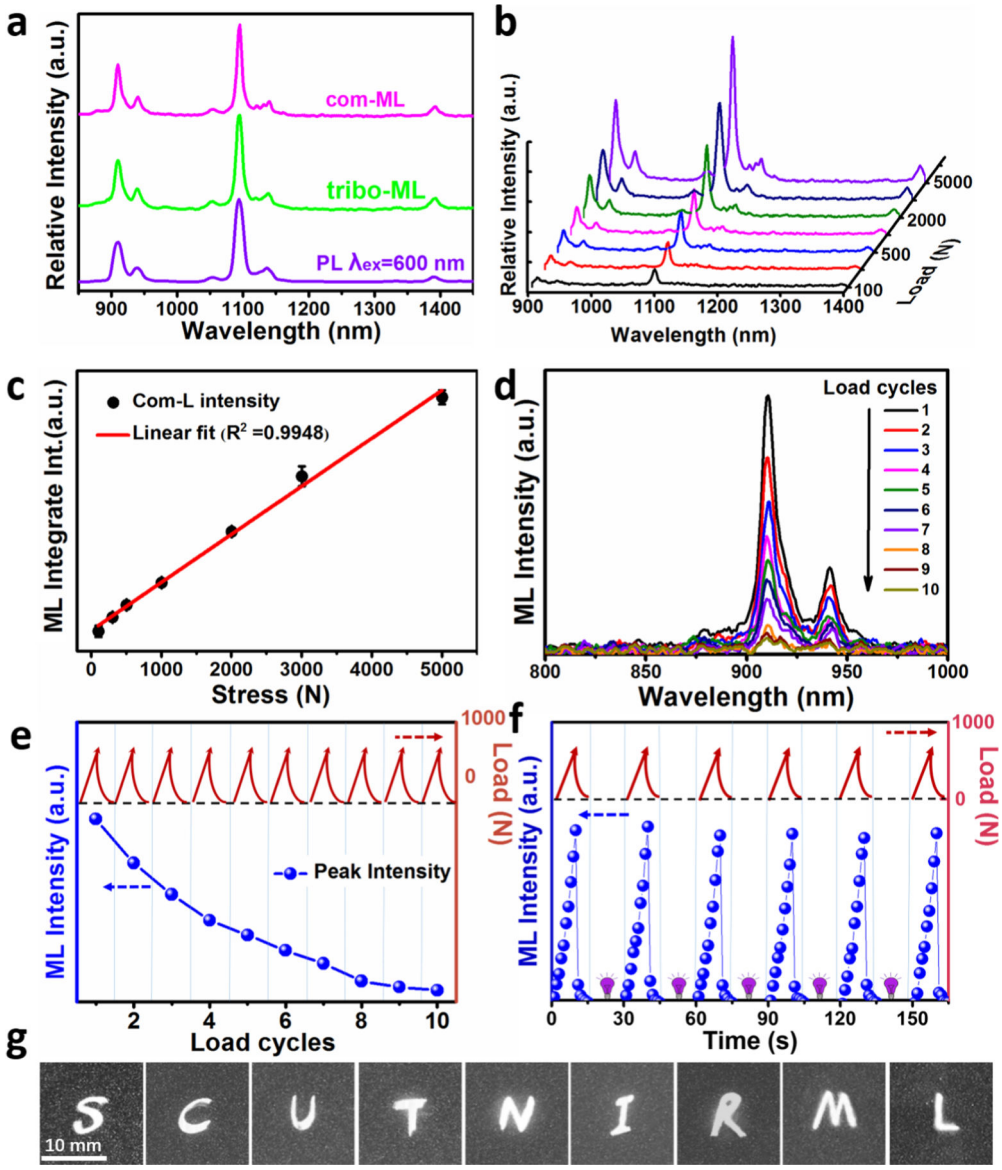

Figure 2.

Characteristics of luminescence under various ways of excitation. (a) Emission spectra of sample CaZnOS:0.5% Nd^{3+} upon excitations by compression (blue line), friction (solid line), and 600 nm light (red line). These spectra are denoted as com-ML, tribo-ML, and PL, respectively. (b) Com-ML spectra of CaZnOS:0.5% Nd^{3+} dispersed into resin as a function of loading forces. (c) Integrated intensity of com-ML (880−1420 nm) as a function of loading forces. (d) Variation in com-ML integrated intensity (bottom) during cyclic loading between 0 and 1000 N (top). (e) NIR ML intensity decay curve under consecutive load cycles. (f) NIR ML recovery behavior after UV irradiation. (g) IR photographs of handwriting on the same spot of a sintered phosphor wafer as recorded with an infrared camera. Exposure time is 2 s.

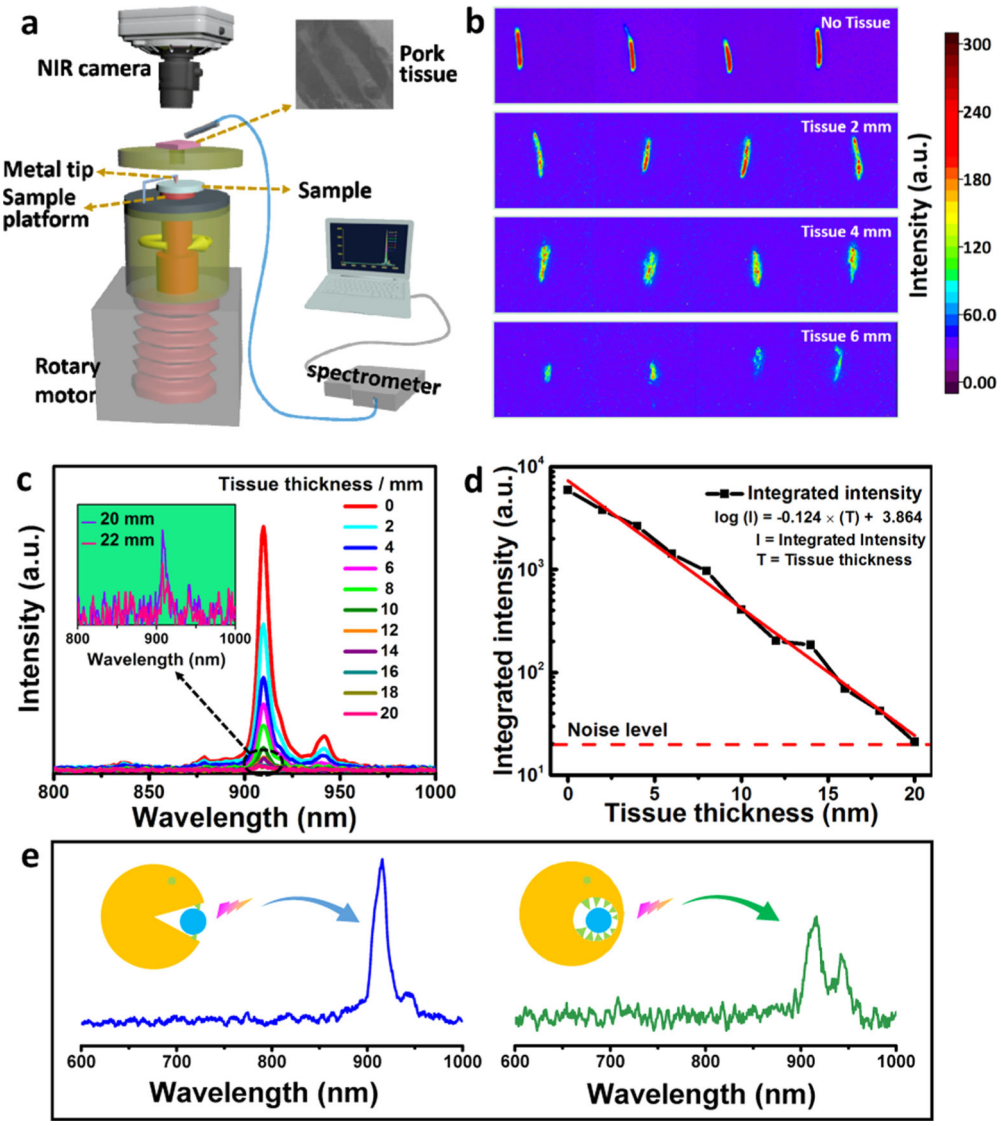

Figure 3.

Demonstration of bioimaging with CaZnOS:1% Nd^{3+}. (a) The schematic diagram for imaging and spectroscopic detection of the NIR EML generated from CaZnOS:Nd^{3+} after passing through the tissue. (b) Bioimaging of tissues by detecting NIR EML light of CaZnOS:Nd^{3+} passing through the tissues with different thicknesses. (c) Emission spectra of NIR EML of CaZnOS:Nd^{3+} passing through the tissues with different thicknesses. Inset: emission spectra corresponding to tissue thickness of 20 and 22 mm. (d) Tissue thickness-dependent log of integrated transmitted emission intensity. Red dash line shows the noise level, whereas red solid line shows the fitted results using a linear equation $\log(I) = -0.124T + 3.864$, where I and T denote the integrated intensity and tissue thickness, respectively. (e) NIR ML signal from the sample bitten by human teeth with mouth open (left) or mouth closed (right), showing that the NIR ML signal can be generated due to teeth biting and still be detected with closed mouth due to good tissue penetration capability.

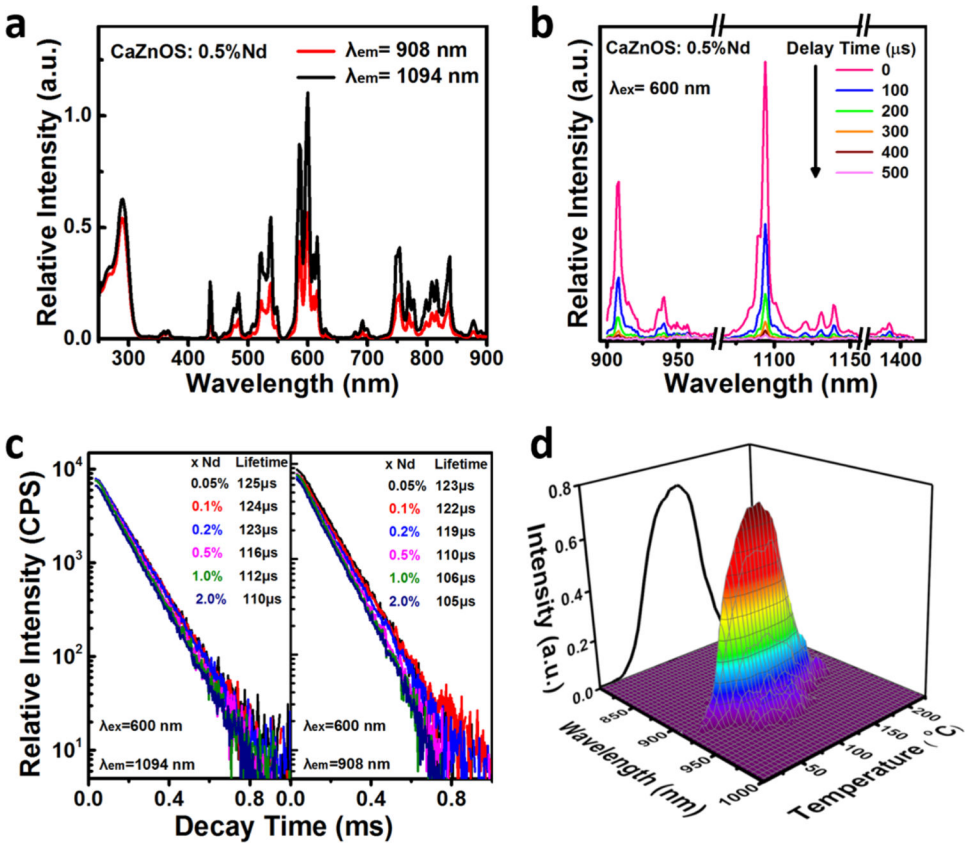

Figure 4.

PL and ThL spectra of CaZnOS:Nd^{3+}. (a) Excitation (λ_{em} = 908 and 1094 nm) and (b) time-resolved emission spectra of CaZnOS:0.5% Nd^{3+} (λ_{ex} = 600 nm); the spectra recorded at different delay times are distinguished by different colors, as labeled in the top right corner. (c) Decay curves of CaZnOS:xNd^{3+} for the peak at 1094 nm (left) and 908 nm (right). The corresponding lifetime at a specific dopant concentration is shown at the top right corner. (d) 3D ThL emission spectrum of CaZnOS:0.5% Nd^{3+}.

Table 1.

ML and PL Properties in RE^{3+}-Doped Phosphors[a]

		visible main peaks (nm)		NIR main peak (nm)	
host	**dopant**	**PL**	**ML**	**PL**	**ML**
CaZnOS	Nd^{3+}			~908	~908
				~1094	~1094
				~1390	~1390
	Pr^{3+}	~519	~519	~1024	No
		~671	~671	~1080	
	Ho^{3+}	~559	~559	~1051	No
		~757	~757	~1200	
	Dy^{3+}	~488	~484	~1029	No
		~574	~574		
		~669	~669		
		~754	~754		
		~852	~852		
$SrAl_20_4$	Nd^{3+}			~890	No
				~1062	
				~1337	
$SrSnO_3$	Nd^{3+}				No

[a]"No" means no emission was detected in ML tests.